Immune Landscape of Colorectal Cancer Tumor Microenvironment from Different Primary Tumor Location

Longhui Zhang[1], Yuetao Zhao[1], Ying Dai[1], Jia-Nan Cheng[1], Zhihua Gong[1], Yi Feng[1], Chengdu Sun[1], Qingzhu Jia[1]* and Bo Zhu[1,2]*

[1]Institute of Cancer, Xinqiao Hospital, Army Medical University, Chongqing, China, [2]Chongqing Key Laboratory of Tumor Immunotherapy, Chongqing, China

To define differences in tumor microenvironment (TME) immune phenotypes between right and left colorectal cancers (CRCs) and explore their therapeutic implications. Gene expression profiling and clinical characteristics of patients with CRC were retrieved from The Cancer Genome Atlas data portal. Immune cell infiltration was estimated based on single-sample gene set enrichment analysis. CRCs tissue microarrays (TMAs) containing 90 consecutive cases of surgical samples were used for validation. Expression of CD8A and VEGFA was confirmed by immunohistochemistry (IHC) analysis with TMAs, and overall survival (OS) was analyzed. Expression profiling data demonstrated that CRC immune microenvironment from right side tumor was characterized as increased infiltration of immune cells with enhanced cytotoxic function, based on higher cytotoxic activity scores (CYT) and interferon-γ signatures. Expression of VEGFA, which could be neutralized by bevacizumab, was associated with decreased levels of activated CD8+ T-cells, Th1 cells, and PRF1 expression on the right side, but not on the left side. IHC analysis of TMAs further confirmed an inverse correlation between CD8A and VEGFA expression, and revealed a favorable OS for patients with CD8A^{Hi}VEGFA^{Lo} disease among right-side CRCs. For the left side, higher CD56^{bright} natural killer cell infiltration and active 4-1BB/IFN-α signaling, which could providing a favorable condition for cetuximab-mediated antibody-dependent cell-mediated cytotoxicity effect, was present in a cohort with extended OS. In the TME, features of immune phenotype sidedness were identified, providing an implication for differential responses to bevacizumab/cetuximab treatment. In addition, a new avenue for innovative experimental design and combinational immunotherapy to treat CRC patients was suggested.

Keywords: right-side colon cancer, left-side colorectal cancer, tumor microenvironment, immunophenotype, therapeutic implications

INTRODUCTION

Colorectal cancer (CRC) is one of the leading causes of cancer mortality worldwide (1). Growing evidence suggests that CRC should be considered a heterogeneous disease; specifically, proximal (cecum to transverse colon) and distal (splenic flexure to rectum) CRC show various biological and clinical differences including embryonic origin, vascular supply, and main physiologic

function (2), which affects disease prognosis (3). Moreover, a series of clinic trials and pooled analysis (4–7) have shown that the location of the primary tumor can be both predictive and prognostic regarding the response to anti-EGFR and anti-angiogenic agents in metastatic colorectal cancer (mCRC). The strongest evidence for the predictive value of primary tumor sidedness and response to EGFR inhibitors is in the first-line treatment of patients in the phase III CALGB/SWOG 80405 trial. The study showed that patients with all RAS wild-type, right-sided primary tumors had longer overall survival (OS) if treated with bevacizumab than if treated with cetuximab in first line, whereas patients with all RAS wild-type, left-sided primary tumors had longer OS if treated with cetuximab than if treated with bevacizumab (5). Specifically, worse prognosis is associated with right-side tumors, when compared with that with left-side tumors, in patients with RAS wild-type mCRC (5, 6). Accordingly, for right-side mCRC, chemotherapy plus bevacizumab seems to be a treatment option. However, the underlying mechanism through which CRC location differentially affects the response to anti-EGFR or anti-angiogenic therapies remains unknown.

Increasing evidence suggests that tumor progression and recurrence are not only governed by the genetic changes inherent to cancer cells but also by tumor microenvironment (TME) factors (8–10). Numerous studies have confirmed that immune cells in the TME modulate cancer progression and are attractive therapeutic targets (11–13). Moreover, the effects of infiltrating immune cells on prognosis have been extensively reported (14–16). Accordingly, we propose that right- and left-side CRC have different immune landscapes, and further, different immune landscape might lead to different prognoses and treatment responses. In this study, we comprehensively compared differences in the immune landscapes between right- and left-side CRCs. To some extent, our findings explain the discrepancies in the prognoses and responses to anti-VEGF and anti-EGFR agents that occur with different primary CRC locations (5, 17, 18). Moreover, the present findings suggest a novel combinational immunotherapy strategy for CRCs of different locations.

MATERIALS AND METHODS

Data Sources

The RSEM-normalized RNA-Seq or microarray datasets for the The Cancer Genome Atlas (TCGA) colon adenocarcinoma (COAD, $n = 467$) cohort and rectum adenocarcinoma (READ, $n = 172$) cohort were downloaded. In total, 638 CRC patients, for whom transcriptome profiling data and clinical characteristics were available, were enrolled in this study. In addition, TCGA data sets and Molecular Signature Database (MSigDB) gene sets were downloaded from https://genome-cancer.ucsc.edu and the Gene Set Enrichment Analysis browser, respectively. The study involved mutation annotation files (MutSig 2.0) that were acquired from the Broad Institute TCGA GDAC Firehose's analysis-2015-04-02.[1]

Gene Signatures

We adopted a previously described procedure to determine the infiltration of immune cells in COAD/READ (19). We obtained the marker gene set for immune cell types from Bindea et al. (20). To calculate single-sample gene set enrichment, we used the GSEA program to derive the absolute enrichment scores of previously experimentally validated gene signatures.

Implementation of Single-Sample Gene Set Enrichment Analysis (ssGSEA)

In brief, the infiltration levels of immune cell types were quantified by ssGSEA in R package gsva. The ssGSEA applies gene signatures expressed by immune cell populations (20) to individual cancer samples (21). The deconvolution approach used in our study included 27 immune cells that are involved in innate immunity [natural killer (NK) cells, CD56^{dim} NK cells, CD56^{bright} NK cells, plasmacytoid dendritic cells (DCs), immature DCs, activated DCs, neutrophils, monocytes, mast cells, eosinophils, and macrophages] and in adaptive immunity (immature B cells, activated B cells, central memory CD4^{+} T, effector memory CD4^{+} T-, activated CD4^{+} T, central memory CD8^{+} T, effector memory CD8^{+} T-, activated CD8^{+} T, NK T-, T follicular helper, Tγδ, Th1, Th2, Th17, and Treg). The observation of T-cell infiltration score (TIS) was defined as the average of the standardized values for CD8^{+} T, central memory CD4^{+} T, effector memory CD4^{+} T-, central memory CD8^{+} T, effector memory CD8^{+} T-, Th1, Th2, Th17, and Treg cells. The obtained CYT score rule from the data set of Rooney et al. (22) consisted of cytolytic genes (calculated as geometrical mean of PRF1 and GZMA). The CD8^{+} T/Treg ratio was the digital ratio of ssGSEA scores for these two cell types. Signaling pathway was evaluated based on ssGSEA (23) according to previously report (24). Gene set for "41BB signaling pathway" and "Interferon-a response" was retrieved from MSigDB (25).

Clinical Information

For COAD and READ, we downloaded clinical files from Genomic Data Commons Data Portal.[2] The sample sizes of different types of analysis are different depending on required data availability.

Survival Analysis

Survival outcome analysis modeled results in reference to the patient OS; specifically, events were defined as death by any cause, and time was accurate to the day. p-Values were obtained from univariate Cox proportional-hazards regression models using the R package survival. All Kaplan–Meier survival curves were drawn using the survfit function in the survival package and were plotted together with the x-axis representing time, and ranging from 0 to 4,000 days.

CRC Tissue Microarray (TMA)

The CRC TMAs contained 90 consecutive cases of surgically resected stages I, II, and III CRC. For each case, one core, 1.5 mm in diameter, was taken at random from the tumor, and an additional 1.5-mm diameter core was taken from histologically normal colonic

---

[1]http://gdac.broadinstitute.org/ (Accessed: April 18, 2017).

[2]https://gdc-portal.nci.nih.gov/ (Accessed: April 18, 2017).

mucosa. Whole TMAs were stained using the standard protocol. In brief, antigen retrieval was performed using EDTA, samples were incubated with the following primary antibodies: recombinant mouse monoclonal anti-human CD8 alpha (1:400 dilution, Abcam; ab199016) and recombinant rabbit monoclonal anti-human VEGFA (1:400 dilution, Abcam; ab52917) for 14 h at 4°C. A negative control was performed by omitting the primary antibody.

Measurement of CD8 Alpha Cell Number and VEGFA Density/Area

After staining for CD8 alpha and VEGFA, slides were scanned with a high-resolution scanner (ScanScope XT; Aperio) at 20× magnification. Image analysis software (Image-Pro Plus, version 6.0.0.260) was used to evaluate the number of CD8 alpha cells and density/area of VEGFA. CD8+ T-cells and VEGFA density/area were assessed in three locations for each microarray as follows: the intratumoral compartment (within the tumor cell nests) and within the adjacent stroma (defined as CD8 cells within one tumor cell diameter of the tumor). The total number of CD8+ T-cells and the density/area of VEGFA were determined by combining the counts for the two compartments. Scores were randomly re-examined by the same investigator after a period of time to ensure reproducibility.

Statistical Methods

A two-sided Mann–Whitney was performed with the R functions *wilcox.test* for nonparametric categorical comparisons. Because we know that the ssGSEA scores are approximately normally distributed, two-tailed *t*-tests and one-way ANOVAs were performed for continuous comparisons. The CD8+ T/Treg ratio represents the digital ratio of ssGSEA scores for these two cell types. Unsupervised clustering for tumor samples, immune cell types, and genes was performed by hierarchical clustering with Pearson's correlation coefficients.

RESULTS

Immune Phenotype Landscape in TME From CRCs

Diverse immune cell populations infiltrate the TME and modulate the antitumor response (*via* activation or suppression). To compare immunophenotypes between CRCs from the left and right side, we first assessed the spectrum of immune cell infiltration. The ssGSEA (21) approach was utilized to deconvolve the relative abundance of each cell type based on expression profiling data retrieved from the TCGA database. For this, 638 CRC patients, for whom transcriptome profiling data and clinical characteristics were available, were included in this study. Based on this analysis, we found significant heterogeneity in terms of infiltration of numerous immune cell types among the cohort (**Figure 1A**); this was in accordance with a recent publication reporting tumor-infiltrating lymphocyte subpopulations in CRC (26). To facilitate further characterization, unsupervised clustering was applied to
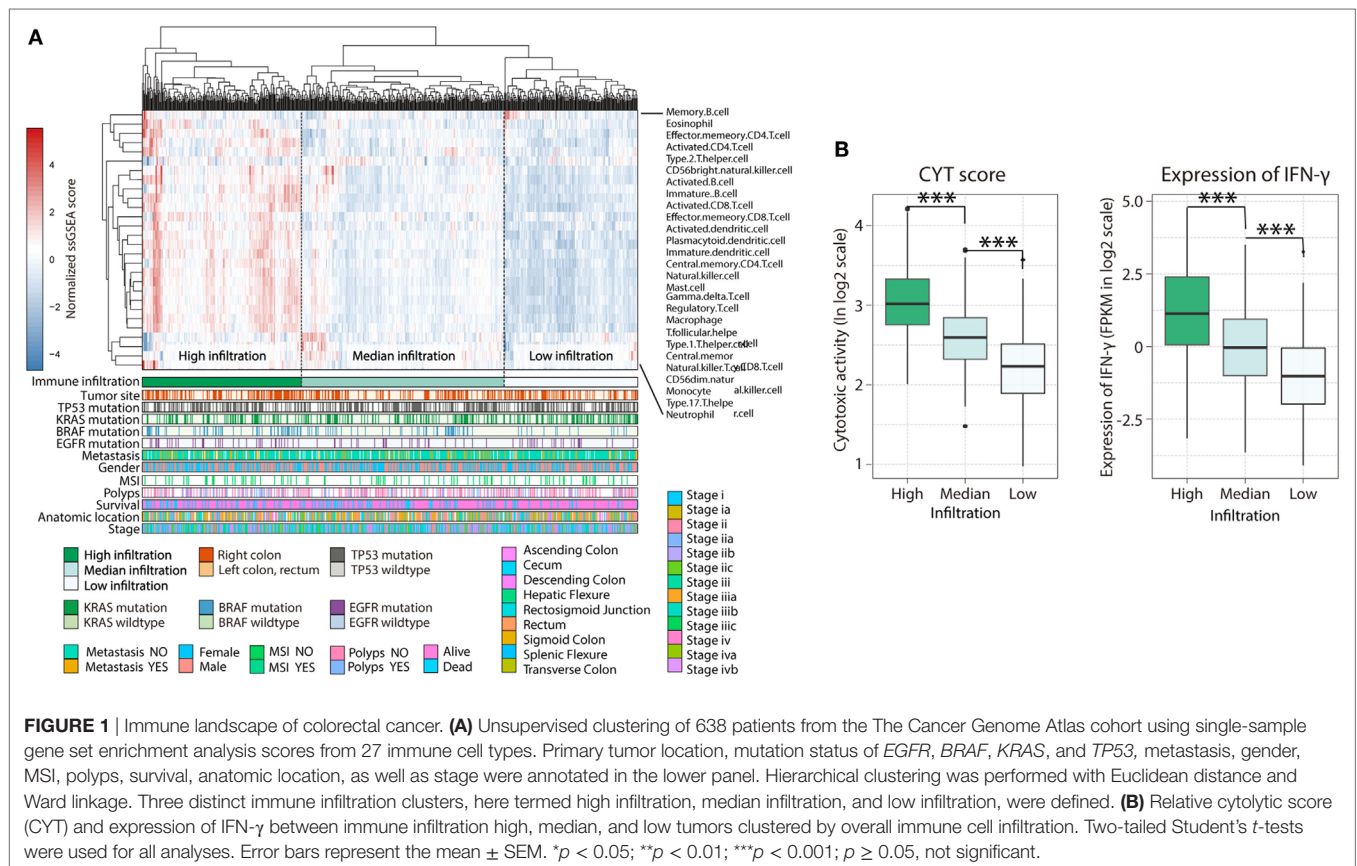
FIGURE 1 | Immune landscape of colorectal cancer. **(A)** Unsupervised clustering of 638 patients from the The Cancer Genome Atlas cohort using single-sample gene set enrichment analysis scores from 27 immune cell types. Primary tumor location, mutation status of *EGFR*, *BRAF*, *KRAS*, and *TP53*, metastasis, gender, MSI, polyps, survival, anatomic location, as well as stage were annotated in the lower panel. Hierarchical clustering was performed with Euclidean distance and Ward linkage. Three distinct immune infiltration clusters, here termed high infiltration, median infiltration, and low infiltration, were defined. **(B)** Relative cytolytic score (CYT) and expression of IFN-γ between immune infiltration high, median, and low tumors clustered by overall immune cell infiltration. Two-tailed Student's *t*-tests were used for all analyses. Error bars represent the mean ± SEM. *$p < 0.05$; **$p < 0.01$; ***$p < 0.001$; $p \geq 0.05$, not significant.

categorize the cohort into three infiltration subgroups—termed high (H, $n = 214$), median (M, $n = 261$), and low (L, $n = 163$) infiltration. Considering the concomitant infiltration of activating and suppressive immune cell types, we investigated whether higher immune cell infiltration correlated with elevated levels of cytotoxic function. To this end, cytolytic activity (CYT), which can serve as a surrogate index for quantifying the magnitude of antitumor response (22), and the expression of IFN-γ, an effector molecule released by activated T-cells, was examined. Patients with high infiltration status showed the highest IFN-γ expression and CYT scores, both indicating that cytotoxic function was efficiently elicited in those patients (**Figure 1B**). In our study, we followed inclusion criteria from several key clinical trials, such as CRYSTAL, FIRE-3, and PRIME (17, 27) to differentiate between the right (cecum to transverse colon) and left (splenic flexure to rectum) CRC with the splenic flexure; we treated rectum cancer as left-side CRC. Furthermore, we analyzed our data using only the non-rectal tissue and found that the immune landscape of the rectum and left-colon cancer microenvironments were not significantly different (Figure S1 in Supplementary Material). For this reason, rectum and left-colon cancer were considered as left-side CRC in our subsequent analysis.

The spectrum of somatic mutations in patients with the left- and right-side CRCs is known to be different (28). These preferences led us to test whether the infiltration pattern of immune cells is associated distinct mutations. The association between immune cell infiltration and the mutation status of *EGFR*, *BRAF*, *KRAS*, and *TP53* was assessed. More infiltration was observed in patients harboring mutations in *EGFR* (Figure S2A in Supplementary Material, H = 169; M = 235; L = 148 vs H = 26; M = 36; L = 24, *EGFR*-mutant vs non-mutant; $p = 0.045$) and *BRAF* (Figure S2B in Supplementary Material, H = 158; M = 214; L = 151 vs H = 47; M = 54; L = 14, $p = 0.0008$), supporting a genomic-immunophenotype correlation found in a recent analysis of melanoma (29). However, there was no relationship between *KRAS* or *TP53* mutation status and immune cell infiltration (Figures S3C,D in Supplementary Material). Consequently, the heterogeneous infiltration of immune cells and its correlation with genomic aberrations suggest that there are different immunophenotypes among patients with distinct primary tumor locations (PTLs).

The Right-Side TME Is Associated With Increased Immune Cell Infiltration and Highly Cytotoxic Potential
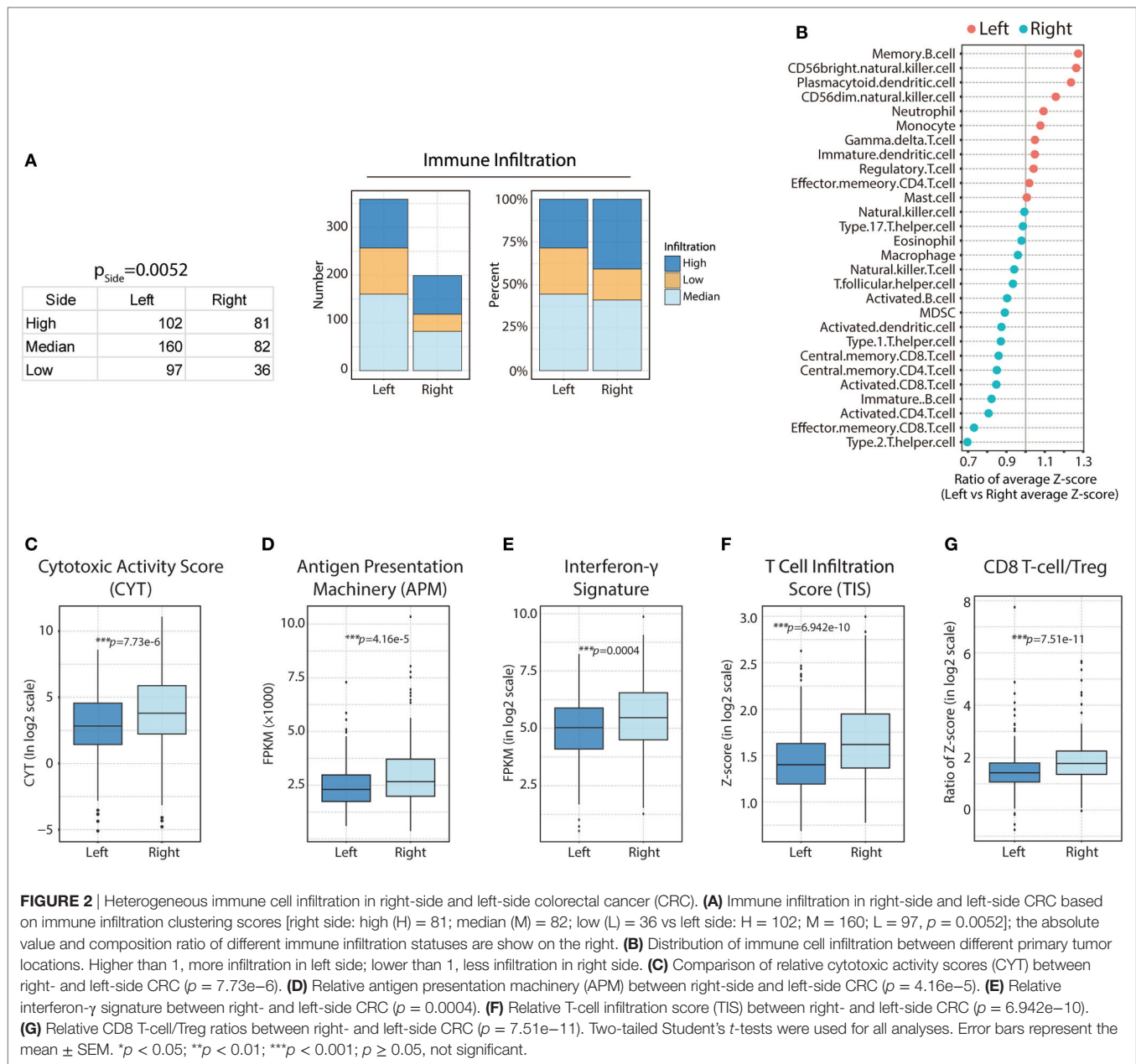
First, we compared total immune cell infiltration among CRCs from different PTLs. Interestingly, we found that the degree of immune infiltration was higher in right-side colon cancer than in left-side CRC (**Figure 2A**; H = 81, M = 82, L = 36 in right side vs H = 102, M = 160, L = 97 in left side; $p = 0.0052$). For more sophisticated characterization, we compared each immune cell population based on their normalized ssGSEA score. Generally, subpopulations of T lymphocytes were found to be predominantly enriched in the TME from the right side, with the exception of effector memory CD4+ T-cells (**Figure 2B**). The association between the enrichment of T lymphocytes based on sidedness and higher immune cell infiltration was corroborated; specifically, enhanced cytotoxic function was identified in patients with

higher immune cell infiltration (**Figure 1B**), suggesting highly cytotoxic potential in right-side tumors. To compare cytotoxic function between PTLs, the associated signatures were identified for each patient. Consistent with the higher infiltration of immune cells, right-side colon cancers were associated with higher levels of immune activation; specifically, cytotoxic activity score (CYT, $p = 7.73e-6$) (**Figure 2C**), antigen presentation machinery (APM, $p = 4.16e-5$) (**Figure 2D**), interferon-γ signature ($p = 0.0004$) (**Figure 2E**), TIS ($p = 6.942e-10$) (**Figure 2F**), and CD8+ T-cell/Treg ratio ($p = 7.51e-11$) were higher (**Figure 2G**). These data illustrate that compared with left-side tumors, right-side tumors have a distinct immune phenotype, characterized by more immune infiltration and higher levels of immune activation.

Enhanced CD56bright NK Cell Response in Left-Side CRC

Natural killer cells are effector lymphocytes of the innate immune system that control several types of tumors by limiting their growth and dissemination (30). In murine models, it has been shown that NK cells can control both local tumor growth and metastasis due to their ability to exert direct-cellular cytotoxicity, without prior sensitization, and to secrete immunostimulatory cytokines like IFN-γ, which helps to shape the immune TME by activating effectors of adaptive immunity (31). Nevertheless, NK cells display impaired functionality and capacity to infiltrate tumors in cancer patients. This suggests that NK cells are feasible targets for immunotherapeutic approaches such as antibody-based strategies (32).

In this study, we determined that left-side CRC was associated with higher levels of CD56bright NK cell infiltration, compared with that in right-side colon cancer (left vs right, $p = 0.012$; **Figure 3A**). More strikingly, CD56bright NK cell infiltration correlated strongly with patient survival in left-side CRC (left $p = 0.0225$; right $p = 0.226$; **Figure 3B**). It has been confirmed that CRC prognosis varies significantly based on PTL; patients with left-side tumors experience higher cure rates and superior OS (33). There are many molecular factors believed to contribute to improved survival in left-side CRC, many of which can be attributed to differences in genetic alterations. Our analysis revealed that major differences in immune infiltration, especially CD56bright NK cells in left-side CRC, might also mediate some of these survival differences. Based on the aforementioned results, we hypothesized that enhanced CD56bright NK cell activation and function in left-side CRC might also be beneficial for prolonged patient survival. Therefore, we performed additional analysis to examine whether the 4-1BB and interferon-α signaling pathways, which are known to reinforce the function of NK cells (34, 35), could also prolong OS for left-side CRCs. As expected, we observed significantly increased survival in patients with more active 4-1BB and interferon-α signaling pathways in left-side CRCs (**Figure 3C**; 4-1BB: $p = 0.00427$, IFNA: $p = 0.0187$ for left side and 4-1BB: $p = 0.961$, IFNA: $p = 0.549$ for right side). Furthermore, to test if higher levels of CD56bright NKs and more active 4-1BB/interferon-α signaling could classify populations based on the best tumor control and extended survival, we performed survival analysis. We identified the most favorable OS in the NKHi41BBHi and NKHiIFNAHi cohort, further implying a critical role of NK subsets
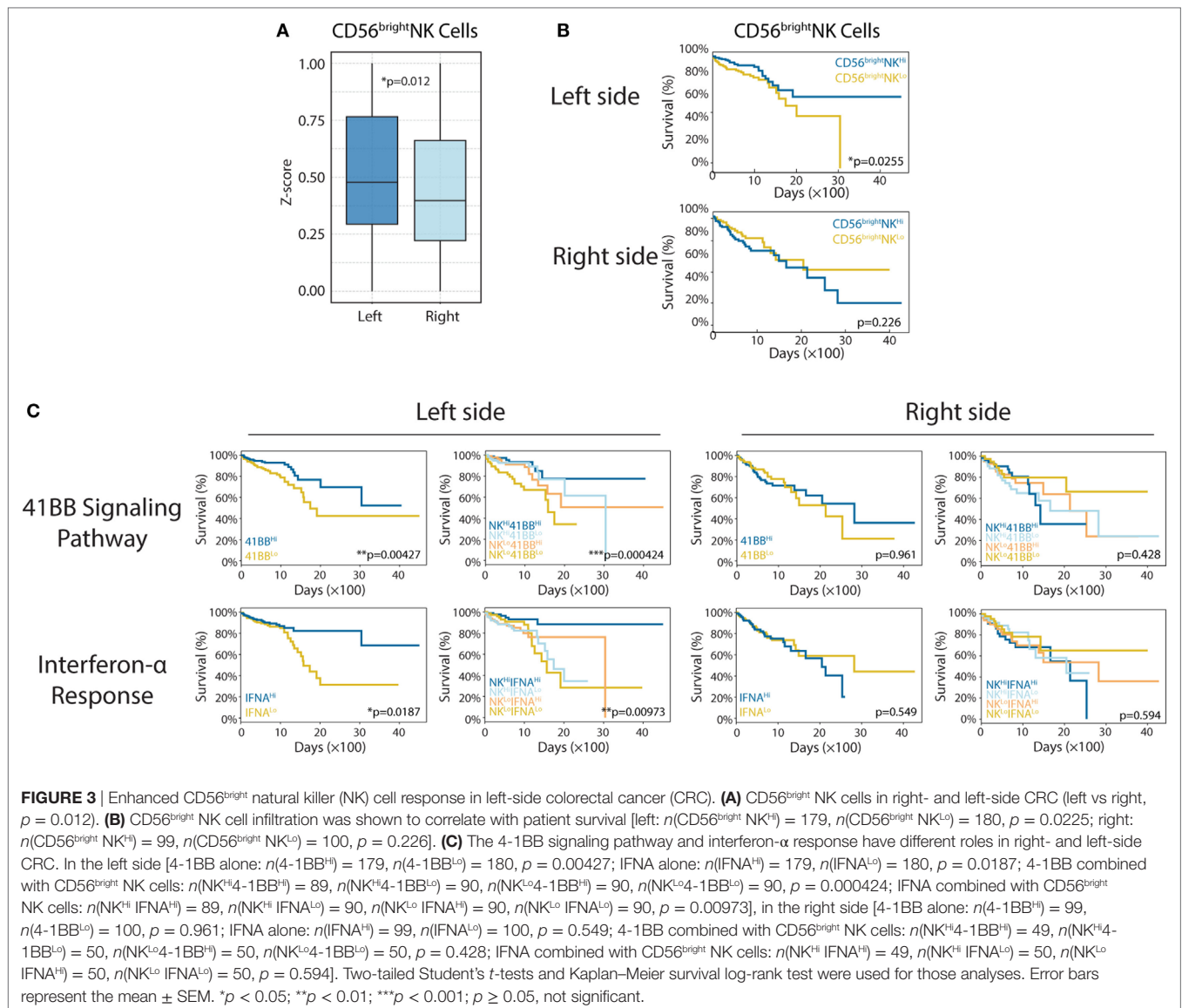
FIGURE 2 | Heterogeneous immune cell infiltration in right-side and left-side colorectal cancer (CRC). **(A)** Immune infiltration in right-side and left-side CRC based on immune infiltration clustering scores [right side: high (H) = 81; median (M) = 82; low (L) = 36 vs left side: H = 102; M = 160; L = 97, p = 0.0052]; the absolute value and composition ratio of different immune infiltration statuses are show on the right. **(B)** Distribution of immune cell infiltration between different primary tumor locations. Higher than 1, more infiltration in left side; lower than 1, less infiltration in right side. **(C)** Comparison of relative cytotoxic activity scores (CYT) between right- and left-side CRC (p = 7.73e−6). **(D)** Relative antigen presentation machinery (APM) between right-side and left-side CRC (p = 4.16e−5). **(E)** Relative interferon-γ signature between right- and left-side CRC (p = 0.0004). **(F)** Relative T-cell infiltration score (TIS) between right- and left-side CRC (p = 6.942e−10). **(G)** Relative CD8 T-cell/Treg ratios between right- and left-side CRC (p = 7.51e−11). Two-tailed Student's t-tests were used for all analyses. Error bars represent the mean ± SEM. *p < 0.05; **p < 0.01; ***p < 0.001; p ≥ 0.05, not significant.

in antitumor immunity in left-side CRC (**Figure 3C**; CD56^{bright} NK cells combined with 4-1BB pathway, p = 0.000424, CD56^{bright} NK cells combined with IFNA pathway, p = 0.00973 for left side and CD56^{bright} NK cells combined with 4-1BB pathway p = 0.428, CD56^{bright} NK cells combined with IFNA pathway p = 0.594).

Vascular Endothelial Growth Factor A (VEGF-A) Is Negatively Related to Cytotoxic Signatures and Predicts OS With CD8 Infiltration in Right-Side CRC

The T-cell immune response is the central event in antitumor immunity. Effective immunotherapy requires that neoantigen-specific T-cells be generated and enter the tumor niche. Pathologic angiogenesis, which is mainly mediated by VEGF-A, prominently hinders T-cell infiltration (36, 37). In this study, we investigated sidedness differences for the correlation between VEGF-A expression and cytotoxicity signatures. For right-side tumors, we found that elevated VEGF-A expression correlated not only with the decreased level of activated CD8$^+$ T-cells (**Figure 4A**, r = −0.267, p = 0.0001) and decreased Th1 cell infiltration (**Figure 4B**, r = −0.239, p = 0.0007) but also with the downregulation of perforin—a predominant molecular effector of cytotoxic activity (**Figure 4C**, r = −0.187, p = 0.007). At the same time, when this analysis was applied to the left-side type of the disease, much weaker correlations were identified, emphasizing the distinct contribution of angiogenesis to impaired infiltration and cytotoxicity (**Figures 4A–C**, red dots and lines). Although the three

FIGURE 3 | Enhanced CD56^bright natural killer (NK) cell response in left-side colorectal cancer (CRC). **(A)** CD56^bright NK cells in right- and left-side CRC (left vs right, $p = 0.012$). **(B)** CD56^bright NK cell infiltration was shown to correlate with patient survival [left: n(CD56^bright NK^Hi) = 179, n(CD56^bright NK^Lo) = 180, $p = 0.0225$; right: n(CD56^bright NK^Hi) = 99, n(CD56^bright NK^Lo) = 100, $p = 0.226$]. **(C)** The 4-1BB signaling pathway and interferon-α response have different roles in right- and left-side CRC. In the left side [4-1BB alone: n(4-1BB^Hi) = 179, n(4-1BB^Lo) = 180, $p = 0.00427$; IFNA alone: n(IFNA^Hi) = 179, n(IFNA^Lo) = 180, $p = 0.0187$; 4-1BB combined with CD56^bright NK cells: n(NK^Hi 4-1BB^Hi) = 89, n(NK^Hi 4-1BB^Lo) = 90, n(NK^Lo 4-1BB^Hi) = 90, n(NK^Lo 4-1BB^Lo) = 90, $p = 0.000424$; IFNA combined with CD56^bright NK cells: n(NK^Hi IFNA^Hi) = 89, n(NK^Hi IFNA^Lo) = 90, n(NK^Lo IFNA^Hi) = 90, n(NK^Lo IFNA^Lo) = 90, $p = 0.00973$], in the right side [4-1BB alone: n(4-1BB^Hi) = 99, n(4-1BB^Lo) = 100, $p = 0.961$; IFNA alone: n(IFNA^Hi) = 99, n(IFNA^Lo) = 100, $p = 0.549$; 4-1BB combined with CD56^bright NK cells: n(NK^Hi 4-1BB^Hi) = 49, n(NK^Hi 4-1BB^Lo) = 50, n(NK^Lo 4-1BB^Hi) = 50, n(NK^Lo 4-1BB^Lo) = 50, $p = 0.428$; IFNA combined with CD56^bright NK cells: n(NK^Hi IFNA^Hi) = 49, n(NK^Hi IFNA^Lo) = 50, n(NK^Lo IFNA^Hi) = 50, n(NK^Lo IFNA^Lo) = 50, $p = 0.594$]. Two-tailed Student's t-tests and Kaplan–Meier survival log-rank test were used for those analyses. Error bars represent the mean ± SEM. $^*p < 0.05$; $^{**}p < 0.01$; $^{***}p < 0.001$; $p \geq 0.05$, not significant.

p values are less than 0.01 in right-side tumors, the correlation coefficients displayed are slightly. We therefore suggest that VEGFA negatively and significantly correlates with cytotoxic signatures in the right-side tumors when compared with the left-side.
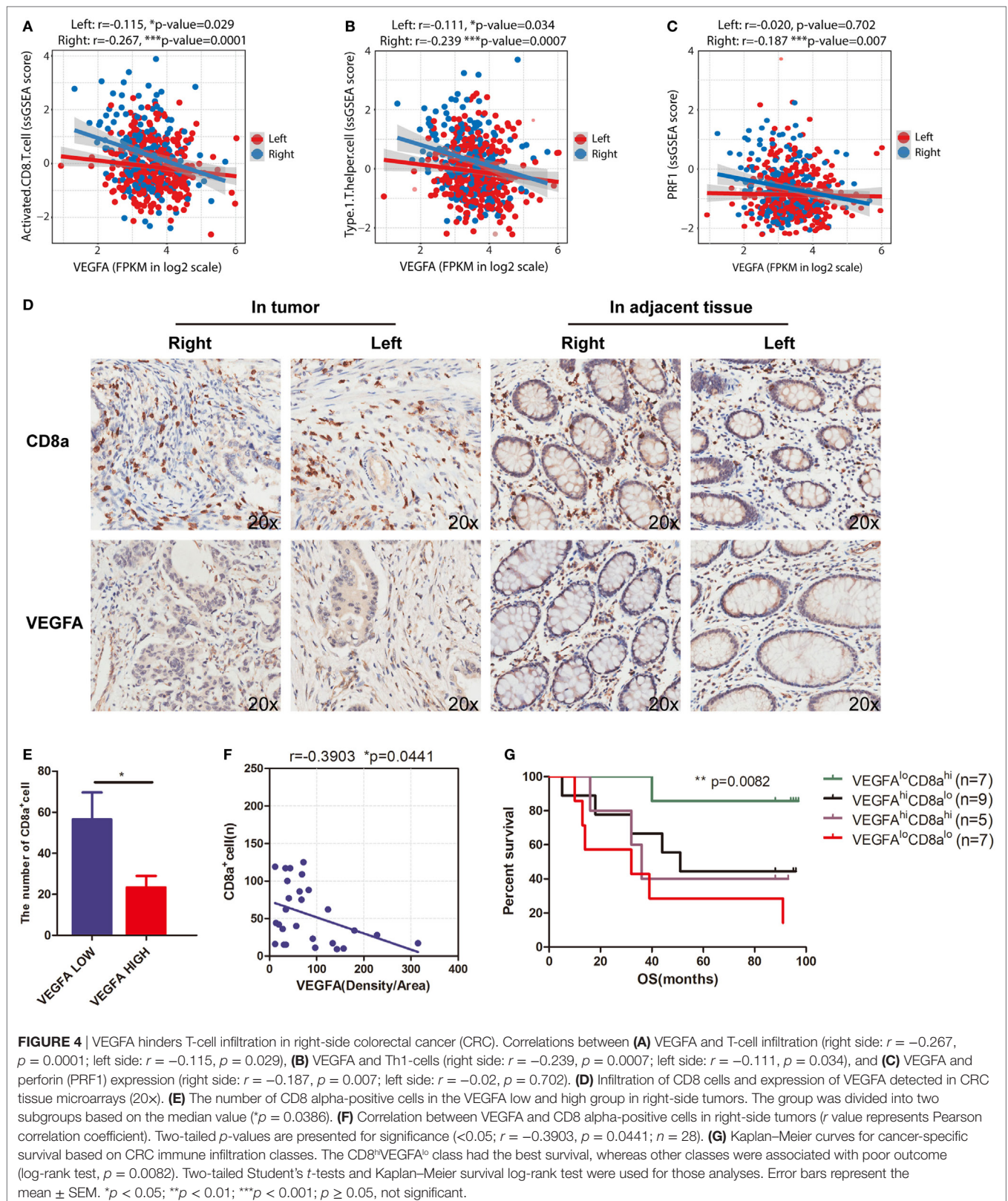
To further validate the findings from TCGA data that VEGFA negatively and significantly correlates with activated CD8^+ T-cell infiltration, we applied immunohistochemical staining of a TMA to analyze a CRC cohort (**Figure 4D**). In the right-side tumor, when patients were grouped based on VEGFA expression, we found a twofold decrease in CD8A expression, and observed a negative correlation ($r = -0.3903$, $^*p = 0.0441$) between VEGFA and CD8A expression in right-side colon cancer (**Figures 4E,F**). This suggests an interaction between VEGFA and CD8^+ T-cells in patients with right-side CRC. This VEGFA-CD8A correlation further leads us to hypothesize a CD8A^Hi VEGFA^Lo cohort with good prognosis among right-side CRCs. As expected, prolonged survival in CD8A^Hi VEGFA^Lo patients was found ($^{**}p = 0.0082$, **Figure 4G**). Taken together, we identified that VEGFA expression

is negatively related to CD8A expression and favorable outcome for CD8A^Hi VEGFA^Lo patients, implying that the antitumor immune microenvironment, and especially the infiltration of CD8^+ T-cells, could feasibly be restored by anti-angiogenic treatment.

DISCUSSION

To the best of our knowledge, this represent the first depiction of the immune landscape of CRCs identified using a large cohort. More importantly, we found that left-side CRC and right-side colon cancer have distinct immune landscapes, and that this immune landscape might, to some extent, explain the primary CRC location-specific differences in prognoses and responses to anti-VEGF and anti-EGFR agents.

In our analysis, we found that there was higher degree of infiltration of the antitumor CD56^bright NK cell subpopulation in left-side CRC. Moreover, CD56^bright NK cell infiltration significantly correlated with patient survival. These findings might explain

FIGURE 4 | VEGFA hinders T-cell infiltration in right-side colorectal cancer (CRC). Correlations between **(A)** VEGFA and T-cell infiltration (right side: $r = -0.267$, $p = 0.0001$; left side: $r = -0.115$, $p = 0.029$), **(B)** VEGFA and Th1-cells (right side: $r = -0.239$, $p = 0.0007$; left side: $r = -0.111$, $p = 0.034$), and **(C)** VEGFA and perforin (PRF1) expression (right side: $r = -0.187$, $p = 0.007$; left side: $r = -0.02$, $p = 0.702$). **(D)** Infiltration of CD8 cells and expression of VEGFA detected in CRC tissue microarrays (20×). **(E)** The number of CD8 alpha-positive cells in the VEGFA low and high group in right-side tumors. The group was divided into two subgroups based on the median value (*$p = 0.0386$). **(F)** Correlation between VEGFA and CD8 alpha-positive cells in right-side tumors (r value represents Pearson correlation coefficient). Two-tailed p-values are presented for significance (<0.05; $r = -0.3903$, $p = 0.0441$; $n = 28$). **(G)** Kaplan–Meier curves for cancer-specific survival based on CRC immune infiltration classes. The CD8^{hi}VEGFA^{lo} class had the best survival, whereas other classes were associated with poor outcome (log-rank test, $p = 0.0082$). Two-tailed Student's t-tests and Kaplan–Meier survival log-rank test were used for those analyses. Error bars represent the mean ± SEM. *$p < 0.05$; **$p < 0.01$; ***$p < 0.001$; $p \geq 0.05$, not significant.

the clinical phenomenon that patients with RAS wild-type, left-sided primary tumors show better response to EGFR inhibitors (cetuximab) than right-sided tumors (FIRE-3 trial) (27). The Fc fragment of cetuximab can bind the Fc receptor FcγRIII (CD16) on NK cells; this initiates a sequence of cellular events culminating in the release of cytotoxic granzyme-containing granules and

INF-γ secretion, which subsequently kills the tumor cells (38). By contrast, we found that activation of the CD137 (4-1BB) receptor signaling pathway was positively associated with patient survival in left-side CRC. This result further supports the recent findings that targeting CD137 enhances cetuximab efficacy (39). More recently, it was found that the PD-1 receptor can also be detected on activated NK cells (40, 41), suggesting that blocking this protein could facilitate CD56^{bright} NK cell cytolytic activity. Therefore, our present findings suggest a new strategy, namely, the combination of anti-PD-L1 antibody with cetuximab, for the treatment of left-side, RAS wild-type CRC. Meanwhile, in the part of survival analysis, we only took into account the effect of NK on OS. This may potentially circumvent the need to target complex and evolving somatic mutational spectrum, such as EGFR, BRAF, p53 mutation status, and mismatch-repair deficiency.

To the best of our knowledge, the T-cell immune response is the central event in antitumor immunity (42, 43). Fortunately, we observed enhanced CD8^{+} T-cell infiltration, cytotoxic activity, and interferon-γ signature and APM in right-side CRC compared with those in left-side CRC. In some cases, right-side CRC and left-side CRC show various biological and clinical differences including embryonic origin, microbiota burden, vascular supply, and main physiologic function (2), which may affect somatic mutations and immune phenotypes between the two different disease locations. These immune phenotypes are consistent with the established knowledge that more mutations are typically found in right-side disease (44–46). However, whether there exists a different expression profile of MHC class I molecules among patients with distinct PTLs need to be further explored. Moreover, this beneficial CD8^{+} T-cell-mediated antitumor response might be blocked by high concentrations of VEGF-A, which not only mediates immune tolerance but also restricts T-cell infiltration into the tumor (47–49). In addition, an analysis of the genomic and transcriptomic features of metastatic melanoma suggests that angiogenesis is enriched in non-response to anti-PD-1 therapy (50). Taken together, these data reveal the paradoxical observation that despite more efficient CD8^{+} T-cell infiltration, cytotoxic activity, and interferon-γ signature and APM, right-side CRC have worse prognosis.
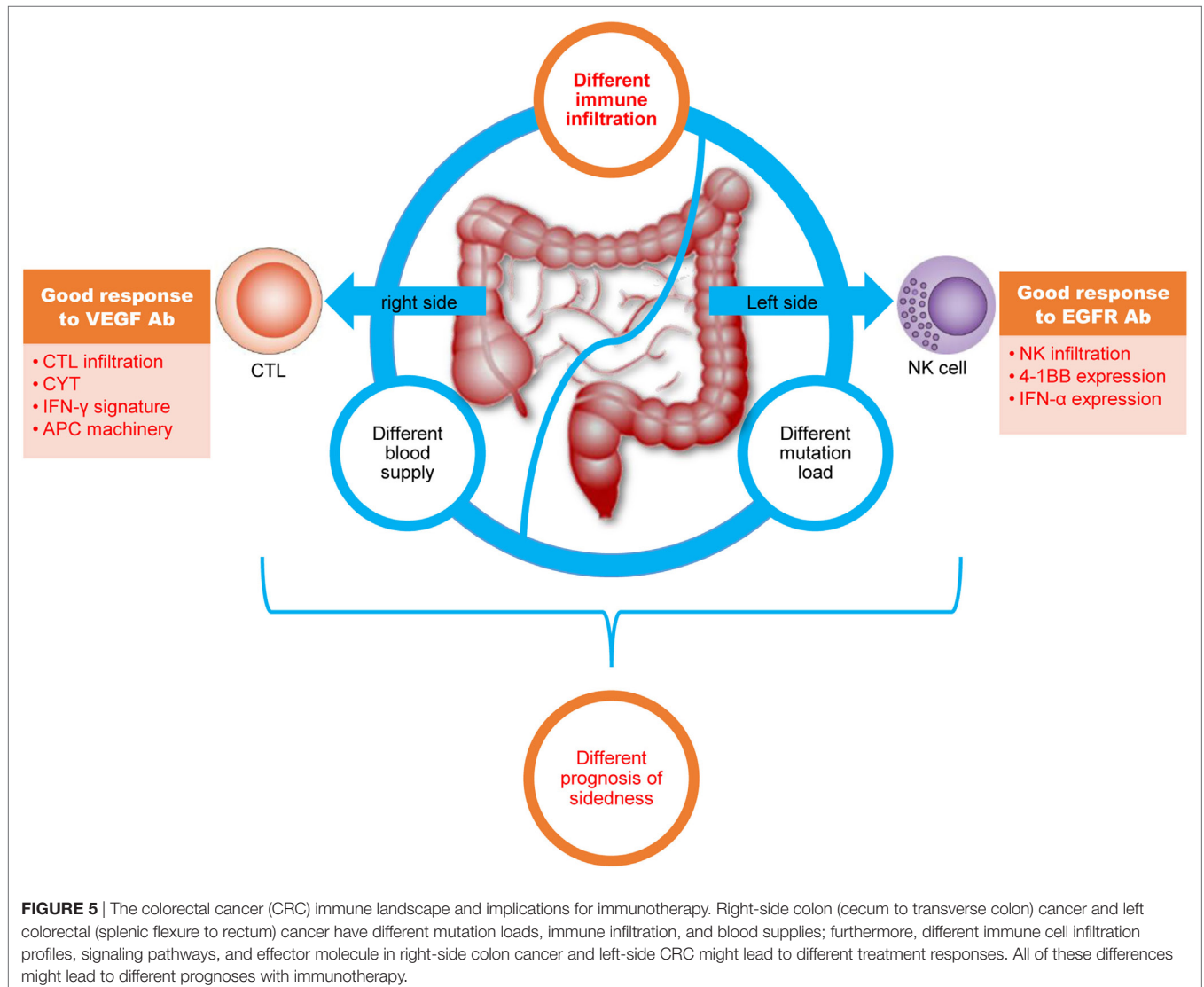

FIGURE 5 | The colorectal cancer (CRC) immune landscape and implications for immunotherapy. Right-side colon (cecum to transverse colon) cancer and left colorectal (splenic flexure to rectum) cancer have different mutation loads, immune infiltration, and blood supplies; furthermore, different immune cell infiltration profiles, signaling pathways, and effector molecule in right-side colon cancer and left-side CRC might lead to different treatment responses. All of these differences might lead to different prognoses with immunotherapy.

Our present results clearly showed that CD8^{+} T-cell infiltration is negatively associated with VEGF-A expression in right-side CRC (**Figure 4A**, $r = -0.267$, $p = 0.0001$). In the analysis of CRC cohort, we also identified that VEGFA is negatively related to CD8A and favorable outcome for CD8A[Hi]VEGFA[Lo] patients. These findings might explain the clinical phenomenon that patients with these primary tumors respond to VEGF inhibitors (bevacizumab) better than those with left-side tumors (PEAK and CALGB/SWOG 80405 trials) [51]. At the same time, tumor display generally higher levels of T cell infiltration but also higher levels of immunoregulatory influence as represented by their PD-1/PD-L1 [52, 53]. In view of these results, we suggest the combination of anti-PD-1 or anti-PD-L1 antibodies and VEGFA inhibition should be of particular interest for the treatment of right-side colon cancer. Coincidentally, the combination of ANGPT2 and VEGFA inhibition and PD-1 blockade was shown to improve tumor control, supporting the rationale for co-targeting angiogenesis and immune checkpoints for colon cancer therapy [54]. Ongoing clinical trials of ANGPT2 and VEGFA inhibitors in combination with the anti-PD-L1 monoclonal antibody atezolizumab (NCT01688206[3]) will provide important information on the benefits of such combination.

Overall, our depiction of the immune landscape of CRC is highly important to clinically relevant processes (**Figure 5**). First, in addition to differences in mutation load and blood supply, we present disparity in immune cell infiltration and immune phenotypes between right- and left-side CRC. These newly identified differences might, to some extent, contribute to the different prognoses between the two different disease locations. Second, predominant CD8^{+} T-cell infiltration in right-side colon cancer and enhanced NK infiltration in left-side CRC explains the elusive clinical phenomenon that patients with right-side disease have good response to anti-VEGFA antibodies, whereas those with left-side CRC have good response to anti-EGFR antibodies. Third, regarding anti-PD-1 or anti-PD-L1 antibody immunotherapy, our results suggest for CRC with wild-type RAS, PD-1/PD-L1 blockage should be combined with anti-VEGF antibodies for right-side disease and with anti-EGFR antibodies for left-side disease.

AUTHOR CONTRIBUTIONS

BZ and QJ conceived and designed the experiments. LZ, YZ, YD, J-NC, ZG, and YF wrote scripts for data analysis. QJ and CS analyzed and interpreted data. QJ and BZ wrote the manuscript.

FUNDING

SUPPLEMENTARY MATERIAL

The Supplementary Material for this article can be found online at https://www.frontiersin.org/articles/10.3389/fimmu.2018.01578/full#supplementary-material.

---

[3] www.clinicaltrials.gov (Accessed: April 18, 2018).

REFERENCES

1. Siegel RL, Miller KD, Jemal A. Cancer statistics, 2016. *CA Cancer J Clin* (2016) 66:7–30. doi:10.3322/caac.21332

2. Minoo P, Zlobec I, Peterson M, Terracciano L, Lugli A. Characterization of rectal, proximal and distal colon cancers based on clinicopathological, molecular and protein profiles. *Int J Oncol* (2010) 37:707–18. doi:10.3892/ijo_00000720

3. Stintzing S, Tejpar S, Gibbs P, Thiebach L, Lenz HJ. Understanding the role of primary tumour localisation in colorectal cancer treatment and outcomes. *Eur J Cancer* (2017) 84:69–80. doi:10.1016/j.ejca.2017.07.016

4. Moretto R, Cremolini C, Rossini D, Pietrantonio F, Battaglin F, Mennitto A, et al. Location of primary tumor and benefit from anti-epidermal growth factor receptor monoclonal antibodies in patients with RAS and BRAF wild-type metastatic colorectal cancer. *Oncologist* (2016) 21:988–94. doi:10.1634/theoncologist.2016-0084

5. Arnold D, Lueza B, Douillard JY, Peeters M, Lenz HJ, Venook A, et al. Prognostic and predictive value of primary tumour side in patients with RAS wild-type metastatic colorectal cancer treated with chemotherapy and EGFR directed antibodies in six randomized trials. *Ann Oncol* (2017) 28:1713–29. doi:10.1093/annonc/mdx175

6. Holch JW, Ricard I, Stintzing S, Modest DP, Heinemann V. The relevance of primary tumour location in patients with metastatic colorectal cancer: a meta-analysis of first-line clinical trials. *Eur J Cancer* (2017) 70:87–98. doi:10.1016/j.ejca.2016.10.007

7. Loree JM, Kopetz S. Recent developments in the treatment of metastatic colorectal cancer. *Ther Adv Med Oncol* (2017) 9:551–64. doi:10.1177/1758834017714997

8. Quail DF, Joyce JA. Microenvironmental regulation of tumor progression and metastasis. *Nat Med* (2013) 19:1423–37. doi:10.1038/nm.3394

9. McAllister SS, Weinberg RA. The tumour-induced systemic environment as a critical regulator of cancer progression and metastasis. *Nat Cell Biol* (2014) 16:717–27. doi:10.1038/ncb3015

10. Barker HE, Paget JT, Khan AA, Harrington KJ. The tumour microenvironment after radiotherapy: mechanisms of resistance and recurrence. *Nat Rev Cancer* (2015) 15:409–25. doi:10.1038/nrc3993

11. Elinav E, Nowarski R, Thaiss CA, Hu B, Jin C, Flavell RA. Inflammation-induced cancer: crosstalk between tumours, immune cells and microorganisms. *Nat Rev Cancer* (2013) 13:759–71. doi:10.1038/nrc3611

12. Topalian SL, Taube JM, Anders RA, Pardoll DM. Mechanism-driven biomarkers to guide immune checkpoint blockade in cancer therapy. *Nat Rev Cancer* (2016) 16:275–87. doi:10.1038/nrc.2016.36

13. Nagarsheth N, Wicha MS, Zou W. Chemokines in the cancer microenvironment and their relevance in cancer immunotherapy. *Nat Rev Immunol* (2017) 17:559–72. doi:10.1038/nri.2017.49

14. Atreya I, Neurath MF. Immune cells in colorectal cancer: prognostic relevance and therapeutic strategies. *Expert Rev Anticancer Ther* (2008) 8:561–72. doi:10.1586/14737140.8.4.561

15. Mlecnik B, Tosolini M, Kirilovsky A, Berger A, Bindea G, Meatchi T, et al. Histopathologic-based prognostic factors of colorectal cancers are associated with the state of the local immune reaction. *J Clin Oncol* (2011) 29:610–8. doi:10.1200/JCO.2010.30.5425

16. Fridman WH, Pages F, Sautes-Fridman C, Galon J. The immune contexture in human tumours: impact on clinical outcome. *Nat Rev Cancer* (2012) 12:298–306. doi:10.1038/nrc3245

17. Tejpar S, Stintzing S, Ciardiello F, Tabernero J, Van Cutsem E, Beier F, et al. Prognostic and predictive relevance of primary tumor location in patients with RAS wild-type metastatic colorectal cancer retrospective analyses of the CRYSTAL and FIRE-3 trials. *JAMA Oncol* (2017) 3:194–201. doi:10.1001/jamaoncol.2016.3797

18. Snyder M, Bottiglieri S, Almhanna K. Impact of primary tumor location on first-line bevacizumab or cetuximab in metastatic colorectal cancer. *Rev Recent Clin Trials* (2018) 13:139–49. doi:10.2174/1574887113666180328104109

19. Senbabaoglu Y, Winer AG, Gejman RS, Liu M, Luna A, Ostrovnaya I, et al. The landscape of T cell infiltration in human cancer and its association with antigen presenting gene expression. *biorxiv* (2015) 4(6):737–44. doi:10.1101/025908

20. Bindea G, Mlecnik B, Tosolini M, Kirilovsky A, Waldner M, Obenauf AC, et al. Spatiotemporal dynamics of intratumoral immune cells reveal the immune landscape in human cancer. *Immunity* (2013) 39:782–95. doi:10.1016/j.immuni.2013.10.003

21. Barbie DA, Tamayo P, Boehm JS, Kim SY, Moody SE, Dunn IF, et al. Systematic RNA interference reveals that oncogenic KRAS-driven cancers require TBK1. *Nature* (2009) 462:108–12. doi:10.1038/nature08460

22. Rooney MS, Shukla SA, Wu CJ, Getz G, Hacohen N. Molecular and genetic properties of tumors associated with local immune cytolytic activity. *Cell* (2015) 160:48–61. doi:10.1016/j.cell.2014.12.033

23. Subramanian A, Tamayo P, Mootha VK, Mukherjee S, Ebert BL, Gillette MA, et al. Gene set enrichment analysis: a knowledge-based approach for interpreting genome-wide expression profiles. *Proc Natl Acad Sci U S A* (2005) 102:15545–50. doi:10.1073/pnas.0506580102

24. Benci JL, Xu B, Qiu Y, Wu TJ, Dada H, Twyman-Saint Victor C, et al. Tumor interferon signaling regulates a multigenic resistance program to immune checkpoint blockade. *Cell* (2016) 167:1540–1554.e12. doi:10.1016/j.cell.2016.11.022

25. Liberzon A, Birger C, Thorvaldsdottir H, Ghandi M, Mesirov JP, Tamayo P. The molecular signatures database (MSigDB) hallmark gene set collection. *Cell Syst* (2015) 1:417–25. doi:10.1016/j.cels.2015.12.004

26. Angelova M, Charoentong P, Hackl H, Fischer ML, Snajder R, Krogsdam AM, et al. Characterization of the immunophenotypes and antigenomes of colorectal cancers reveals distinct tumor escape mechanisms and novel targets for immunotherapy. *Genome Biol* (2015) 16:64. doi:10.1186/s13059-015-0620-6

27. Stintzing S, Modest DP, Rossius L, Lerch MM, von Weikersthal LF, Decker T, et al. FOLFIRI plus cetuximab versus FOLFIRI plus bevacizumab for metastatic colorectal cancer (FIRE-3): a post-hoc analysis of tumour dynamics in the final RAS wild-type subgroup of this randomised open-label phase 3 trial. *Lancet Oncol* (2016) 17:1426–34. doi:10.1016/S1470-2045(16)30269-8

28. Missiaglia E, Jacobs B, D'Ario G, Di Narzo AF, Soneson C, Budinska E, et al. Distal and proximal colon cancers differ in terms of molecular, pathological, and clinical features. *Ann Oncol* (2014) 25:1995–2001. doi:10.1093/annonc/mdu275

29. Charoentong P, Finotello F, Angelova M, Mayer C, Efremova M, Rieder D, et al. Pan-cancer immunogenomic analyses reveal genotype-immunophenotype relationships and predictors of response to checkpoint blockade. *Cell Rep* (2017) 18:248–62. doi:10.1016/j.celrep.2016.12.019

30. Vivier E, Tomasello E, Baratin M, Walzer T, Ugolini S. Functions of natural killer cells. *Nat Immunol* (2008) 9:503–10. doi:10.1038/ni1582

31. Morvan MG, Lanier LL. NK cells and cancer: you can teach innate cells new tricks. *Nat Rev Cancer* (2016) 16:7–19. doi:10.1038/nrc.2015.5

32. Freud AG, Becknell B, Roychowdhury S, Mao HC, Ferketich AK, Nuovo GJ, et al. A human CD34(+) subset resides in lymph nodes and differentiates into CD56bright natural killer cells. *Immunity* (2005) 22:295–304. doi:10.1016/j.immuni.2005.01.013

33. Loupakis F, Yang D, Yau L, Feng S, Cremolini C, Zhang W, et al. Primary tumor location as a prognostic factor in metastatic colorectal cancer. *J Natl Cancer Inst* (2015) 107(3):dju427. doi:10.1093/jnci/dju427

34. Srivastava RM, Trivedi S, Concha-Benavente F, Gibson SP, Reeder C, Ferrone S, et al. CD137 stimulation enhances cetuximab-induced natural killer: dendritic cell priming of antitumor T-cell immunity in patients with head and neck cancer. *Clin Cancer Res* (2017) 23:707–16. doi:10.1158/1078-0432.CCR-16-0879

35. Shen X, Fu B, Liu Y, Guo C, Ye Y, Sun R, et al. NKp30+ NK cells are associated with HBV control during pegylated-interferon-alpha-2b therapy of chronic hepatitis B. *Sci Rep* (2016) 6:38778. doi:10.1038/srep38778

36. Ferrara N, Adamis AP. Ten years of anti-vascular endothelial growth factor therapy. *Nat Rev Drug Discov* (2016) 15:385–403. doi:10.1038/nrd.2015.17

37. Muller WA. Mechanisms of leukocyte transendothelial migration. *Annu Rev Pathol* (2011) 6:323–44. doi:10.1146/annurev-pathol-011110-130224

38. Terunuma H, Deng X, Dewan Z, Fujimoto S, Yamamoto N. Potential role of NK cells in the induction of immune responses: implications for NK cell-based immunotherapy for cancers and viral infections. *Int Rev Immunol* (2008) 27:93–110. doi:10.1080/08830180801911743

39. Kohrt HE, Colevas AD, Houot R, Weiskopf K, Goldstein MJ, Lund P, et al. Targeting CD137 enhances the efficacy of cetuximab. *J Clin Invest* (2014) 124:2668–82. doi:10.1172/JCI73014

40. Norris S, Coleman A, Kuri-Cervantes L, Bower M, Nelson M, Goodier MR. PD-1 expression on natural killer cells and CD8(+) T cells during chronic HIV-1 infection. *Viral Immunol* (2012) 25:329–32. doi:10.1089/vim.2011.0096

41. Bellucci R, Martin A, Bommarito D, Wang K, Hansen SH, Freeman GJ, et al. Interferon-γ-induced activation of JAK1 and JAK2 suppresses tumor cell susceptibility to NK cells through upregulation of PD-L1 expression. *Oncoimmunology* (2015) 4:e1008824. doi:10.1080/2162402X.2015.1008824

42. Reading JL, Galvez-Cancino F, Swanton C, Lladser A, Peggs KS, Quezada SA. The function and dysfunction of memory CD8(+) T cells in tumor immunity. *Immunol Rev* (2018) 283:194–212. doi:10.1111/imr.12657

43. Tumeh PC, Harview CL, Yearley JH, Shintaku IP, Taylor EJ, Robert L, et al. PD-1 blockade induces responses by inhibiting adaptive immune resistance. *Nature* (2014) 515:568–71. doi:10.1038/nature13954

44. Tran B, Kopetz S, Tie J, Gibbs P, Jiang ZQ, Lieu CH, et al. Impact of BRAF mutation and microsatellite instability on the pattern of metastatic spread and prognosis in metastatic colorectal cancer. *Cancer* (2011) 117:4623–32. doi:10.1002/cncr.26086

45. Llosa NJ, Cruise M, Tam A, Wicks EC, Hechenbleikner EM, Taube JM, et al. The vigorous immune microenvironment of microsatellite instable colon cancer is balanced by multiple counter-inhibitory checkpoints. *Cancer Discov* (2015) 5:43–51. doi:10.1158/2159-8290.CD-14-0863

46. Le DT, Durham JN, Smith KN, Wang H, Bartlett BR, Aulakh LK, et al. Mismatch repair deficiency predicts response of solid tumors to PD-1 blockade. *Science* (2017) 357:409–13. doi:10.1126/science.aan6733

47. Terme M, Pernot S, Marcheteau E, Sandoval F, Benhamouda N, Colussi O, et al. VEGFA-VEGFR pathway blockade inhibits tumor-induced regulatory T-cell proliferation in colorectal cancer. *Cancer Res* (2013) 73:539–49. doi:10.1158/0008-5472.CAN-12-2325

48. Huang H, Langenkamp E, Georganaki M, Loskog A, Fuchs PF, Dieterich LC, et al. VEGF suppresses T-lymphocyte infiltration in the tumor microenvironment through inhibition of NF-kB-induced endothelial activation. *FASEB J* (2015) 29:227–38. doi:10.1096/fj.14-250985

49. Voron T, Colussi O, Marcheteau E, Pernot S, Nizard M, Pointet AL, et al. VEGF-A modulates expression of inhibitory checkpoints on CD8+ T cells in tumors. *J Exp Med* (2015) 212:139–48. doi:10.1084/jem.20140559

50. Hugo W, Zaretsky JM, Sun L, Song C, Moreno BH, Hu-Lieskovan S, et al. Genomic and transcriptomic features of response to anti-PD-1 therapy in metastatic melanoma. *Cell* (2016) 165:35–44. doi:10.1016/j.cell.2016.02.065

51. O'Keefe SJ. Diet, microorganisms and their metabolites, and colon cancer. *Nat Rev Gastroenterol Hepatol* (2016) 13:691–706. doi:10.1038/nrgastro.2016.165

52. Chen YP, Zhang J, Wang YQ, Liu N, He QM, Yang XJ, et al. The immune molecular landscape of the B7 and TNFR immunoregulatory ligand-receptor families in head and neck cancer: a comprehensive overview and the immunotherapeutic implications. *Oncoimmunology* (2017) 6:e1288329. doi:10.1080/2162402X.2017.1288329

53. Mandal R, Senbabaoglu Y, Desrichard A, Havel JJ, Dalin MG, Riaz N, et al. The head and neck cancer immune landscape and its immunotherapeutic implications. *JCI Insight* (2016) 1:e89829. doi:10.1172/jci.insight.89829

54. Schmittnaegel M, Rigamonti N, Kadioglu E, Cassara A, Wyser Rmili C, Kiialainen A, et al. Dual angiopoietin-2 and VEGFA inhibition elicits antitumor immunity that is enhanced by PD-1 checkpoint blockade. *Sci Transl Med* (2017) 9:eaak9670. doi:10.1126/scitranslmed.aak9670